Optics and Lasers in Engineering 51 (2013) 1321–1326

Contents lists available at SciVerse ScienceDirect

Optics and Lasers in Engineering

journal homepage: www.elsevier.com/locate/optlaseng

Microlenses focal length measurement using Z-scan and parallel moiré deflectometry

Saifollah Rasouli [a,b,c,*], Y. Rajabi [a], H. Sarabi [a]

[a] Department of Physics, Institute for Advanced Studies in Basic Sciences (IASBS), Zanjan 45137-66731, Iran
[b] Optics Research Center, Institute for Advanced Studies in Basic Sciences (IASBS), Zanjan 45137-66731, Iran
[c] The Abdus Salam ICTP, Strada Costiera 11, 34014 Trieste, Italy

ARTICLE INFO

Article history:
Received 9 January 2013
Received in revised form
4 May 2013
Accepted 21 May 2013
Available online 20 June 2013

Keywords:
Parallel moiré deflectometry
Microlens
Effective focal length

ABSTRACT

In this paper, a simple and accurate method based on Z-scan and parallel moiré deflectometry for measuring the focal length of microlenses is reported. A laser beam is focused by one lens and is re-collimated by another lens, and then strikes a parallel moiré deflectometer. In the presence of a microlens near the focal point of the first lens, the radius of curvature of the beam is changed; the parallel moiré fringes are formed only due to the beam divergence or convergence. The focal length of the microlens is obtained from the moiré fringe period graph without the need to know the position of the principal planes. This method is simple, more reliable, and completely automated. The implementation of the method is straightforward. Since a focused laser beam and Z-scan in free space are used, it can be employed for determining small focal lengths of small size microlenses without serious limitation on their size.

1. Introduction

In recent years, microlenses have found wide applications in various fields of science, industry, and military [1,2]. Microlenses are used both individually and as an array, in different applications such as focusing the light into optical fibers, optical fibers connection, collimation of diode lasers, high-quality imaging systems, microscopy and microsystems, spatial filtering, wavefront sensors, LCDs, etc. The most important parameters of a microlens are its focal length and its radius of curvature. Because a microlens has a small size, the determination of its focal length is not straightforward. Therefore, the measurement of the focal length of the microlens is a key factor. There are many methods for characterization of microlenses like digital holographic microscopy [3], Mach–Zehnder interferometry [4], combined Twyman–Green and Mach–Zehnder interferometry [5], interference microscopy [6], and so on [7–9]. All of the mentioned methods need expensive equipment and suffer from environmental vibrations. In addition, the interferometric testing of microlenses incurs certain difficulties due to the small sizes of the microlenses. An undesired diffraction pattern is encountered. Another problem, especially in reflection testing setups, is unwanted reflections from other surfaces than the surface to be tested. On the other hand, the Z-scan technique has been implemented for measuring the nonlinear refractive index of materials, n_2 [10]. The Z-scan technique is also used for measuring the focal length of microlenses [11]. In measuring the n_2 of materials or the focal length of a regular lens, the Z-scan technique has the disadvantage of being sensitive to the beam pointing instability and power fluctuations.

On the other hand, there are various methods for measuring the focal length of ordinary lenses, such as using the interferometry method [12], Talbot interferometry and Talbot effect [13,14], digital speckle interferometry [15], moiré deflectometry [16], Lau effect [17], and Shack–Hartman wavefront sensor [18]. All of the mentioned methods are applicable to large scale lenses.

In this paper, we have used Z-scan and parallel moiré deflectometry for measuring the focal length of microlenses. It should be mentioned that we have previously employed the parallel moiré deflectometry for measuring the atmospheric turbulence parameters [19,20] and refractive index of nonlinear materials [21]. A laser beam is focused by one lens and is re-collimated by another lens, and then strikes a parallel moiré deflectometer. In a parallel moiré deflectometer the grating vectors are parallel, and the resulting moiré fringes are also parallel to the grating lines. In the presence of a microlens near the focal point of the first lens, the radius of curvature of the beam is changed; the parallel moiré fringes are formed only due to the beam divergence or convergence. In the measuring process, the microlens is accurately shifted along the optical axis near the focal point of the first lens using a DC stepper motor. The value of the shift in a step is 1/200 mm. Then the moiré patterns corresponding to the different

* Corresponding author at: Department of Physics, Institute for Advanced Studies in Basic Sciences (IASBS), Zanjan 45137-66731, Iran. Tel.: +98 241 4152012; fax: +98 241 4152104.
E-mail addresses: rasouli@iasbs.ac.ir, rasouli_1379@yahoo.com (S. Rasouli).

0143-8166/$ - see front matter Crown Copyright © 2013 Published by Elsevier Ltd. All rights reserved.
http://dx.doi.org/10.1016/j.optlaseng.2013.05.012

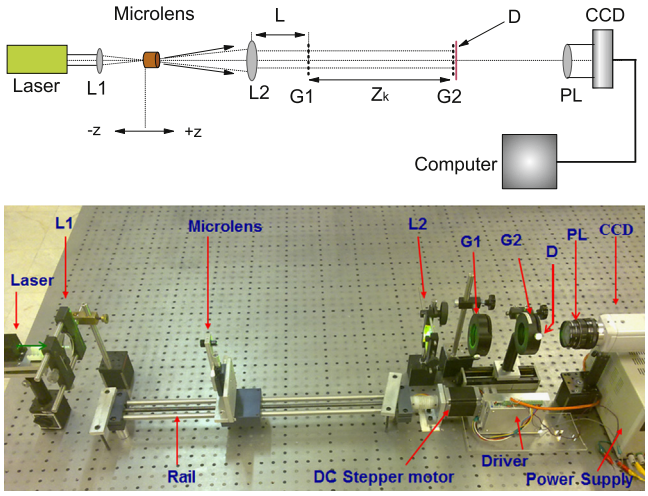

Fig. 1. Top: integrated instrument. Bottom: schematic diagram of the experimental setup. L1, L2, G1, G2, D, PL, and CCD stand for the focusing lens, collimating lens, first grating, second grating, diffuser, projection lens, and scientific camera, respectively.

positions of the microlens are recorded. In this method we measure the radius of the curvature of the laser beam as a function of the microlens position, and the focal length of the microlens is obtained from the moiré fringe period graph without the need to know the position of the principal planes. By selection of a suitable grating period and the distance between the gratings, one can adjust the precision according to the focal length of the microlens.

This method is simple, more reliable and completely automated. The implementation of the method is straightforward. Because only a focused laser beam and Z-scan information are needed, it can be employed for determining small focal lengths of small size microlenses without any limitation on their sizes.

2. Theoretical background

Schematic diagram of the experimental setup is shown in Fig. 1. After propagation through a positive lens, $L1$, the laser beam is re-collimated by the second lens, $L2$. Then the beam illuminates two gratings $G1$ and $G2$ with equal periods of d, separated by Z_k along the optical axis, in which their lines and planes are parallel with each other. The parameter Z_k denotes the kth Talbot's distance for the $G1$. The planes of the gratings are assumed to be perpendicular to the optical axis. The test microlens is placed at the focal plane of $L1$. The displacement of the microlens along the optical axis causes displacement of the location of the focus point of the beam and correspondingly changes the radius of curvature of the beam on $G1$.

In this case, the spatial period of the self-image is magnified by $(r+Z_k)/r$, where r is the radius of curvature of the laser beam at G1 plane. r is positive when the beam on the $G1$ plane is divergent and is negative when it is convergent. On the $G2$ plane, a multiplicative moiré pattern will appear by the superposition of the kth self-image of $G1$, with period $d\pm\delta d$, and $G2$, with period d, where the "+" and the "−" signs correspond to the divergent and convergent beams, respectively. In this case the spatial period of the moiré fringes obtained from [22]

$$d_m=\frac{d^2}{\delta d}, \tag{1}$$

and moiré fringes are parallel to the grating's rulings. More detail and two new applications of this kind of moiré fringes are presented in [19,21]. Using geometrical optics, it is easy to find that [19,21], $(d+\delta d)/d=(Z_k+r)/r$, and as a result one can write

$$\delta d=\frac{Z_k}{|r|}d. \tag{2}$$

Using Eq. (2) in Eq. (1) we get

$$d_m=\frac{|r|d}{Z_k}. \tag{3}$$

As shown, d_m depends on the radius of curvature of the beam.

Any change in the position of the microlens near the focal length of $L1$, causes a change in the radius of curvature of the beam and the period of moiré fringes. Now by using the ray tracing procedure [23], let us describe the propagation of the beam through $L1$ (with focal length f_1), the microlens (with an effective focal length f_{ml}), $L2$ (with focal length f_2) and the distances between the elements. By using the transfer matrices of lenses and the free spaces, the $ABCD$ matrices of the system is given by

$$\begin{pmatrix}A & C\\ B & D\end{pmatrix}=\begin{pmatrix}1 & 0\\ \frac{-1}{f_2} & 1\end{pmatrix}\begin{pmatrix}1 & f_2-z\\ 0 & 1\end{pmatrix}\begin{pmatrix}1 & 0\\ \frac{-1}{f_{ml}} & 1\end{pmatrix}\begin{pmatrix}1 & f_{1+z}\\ 0 & 1\end{pmatrix}\begin{pmatrix}1 & 0\\ \frac{-1}{f_1} & 1\end{pmatrix}. \tag{4}$$

The effective focal length, EFL, of a system is the distance from the principal point to the focal point. The back focal length, BFL, or back focus is the distance from the vertex of the last surface of the system to the second focal point. From the theory of the $ABCD$ matrices the focal length of a system, and the EFL–BFL are given by $f_t=-1/C$, and $S=(1-A)/C$, respectively [23]. According to the configuration of the Fig. 1, radius of curvature of the beam on $G1$ is given by

$$r(z)=L-S(z)-f_t(z), \tag{5}$$

where L is the distance between $L2$ and G1 and $S(z)$ is the distance of exit plane and second principal plane of the complex optical system. After some calculations, we obtain

$$r(z)=L+\frac{f_2^2}{z}-\frac{f_{ml}f_2^2}{z^2}-f_2. \tag{6}$$

Finally combining Eqs. (6) and (3) we have

$$d_m=\left|\frac{d}{Z_k}(L-f_2)+\frac{df_2^2}{zZ_k}\left(1-\frac{f_{ml}}{z}\right)\right|. \tag{7}$$

According to Eq. (7) the period of moiré fringes, d_m, will be infinite, when microlense is placed at the focal point ($z=0$). By measuring the moiré fringe period at various positions of the microlens, using Eq. (7) the focal length of microlens, f_{ml}, is calculated without the need to know the position of the principal planes.

3. Experimental work

The second harmonic of a 50 mW CW diode-pumped Nd-YAG laser beam with a wavelength of 532 nm is collimated by a double lens telescopic system. The collimated and expanded laser beam strike $G1$ with the period of $d=0.1$ mm. The second grating of the moiré deflectometer $G2$ with the same period is installed at a distance of 75 mm with respect to the first grating $G1$.

The gratings $G1$ and $G2$ are installed on suitable mounts. The holders of the gratings can be rotated around the optical axis for adjusting the angle between the grating vectors. The moiré pattern is formed at a plane where the second grating of the moiré deflectometer and a diffuser, D, are installed. Using a projection lens, PL, the moiré pattern is projected on the CCD camera.

The test microlens is installed on a micro-positioner on an optical rail and is accurately shifted along the z direction near the focal point of the first lens using a DC stepper motor. The value of the shift in a step along the z direction is 1/200 mm. It can

displaced in the plane perpendicular to the z direction by the micro-positioner for aligning the microlens' axis on the optical axis of the setup. The moiré fringes corresponding to different positions of the microlens are automatically recorded and stored in a computer.

Figs. 2 and 3 show typical frames of the moiré patterns that were recorded on both sides of the focal point for a 40X objective and for a typical microlens, respectively. We observe that the period of moiré fringes will change when the sample moves between two lenses $L1$ and $L2$.

To get clearer fringes the high frequency illumination of the pattern i.e., the image of the grating lines, is removed by fast Fourier transform using MATLAB software. Details of the fringe analysis are shown in Figs. 4 and 5: in (a)–(d) a typical moiré pattern at a given z, corresponding to low–frequency illumination distribution, and intensity profile along the dashed red line illustrated in (b) are shown. Calculated moiré fringe period at the given z is shown by a blue circle in (d). Other data points in (d) correspond to other values of z. The background movies of Figs. 4 and 5 contain similar data of successive frames recorded in different z.

In Figs. 6 and 7 measured Z-scan values of the period of moiré fringes are plotted for the above mentioned 40X objective and microlens with commercial focal lengths of 4 mm and 16 mm, respectively. For experimental values of $f_2=520$ mm, $f_1=200$ mm, $Z_k=75$ mm, $L=88$ mm, and $d=1/10$ mm the values

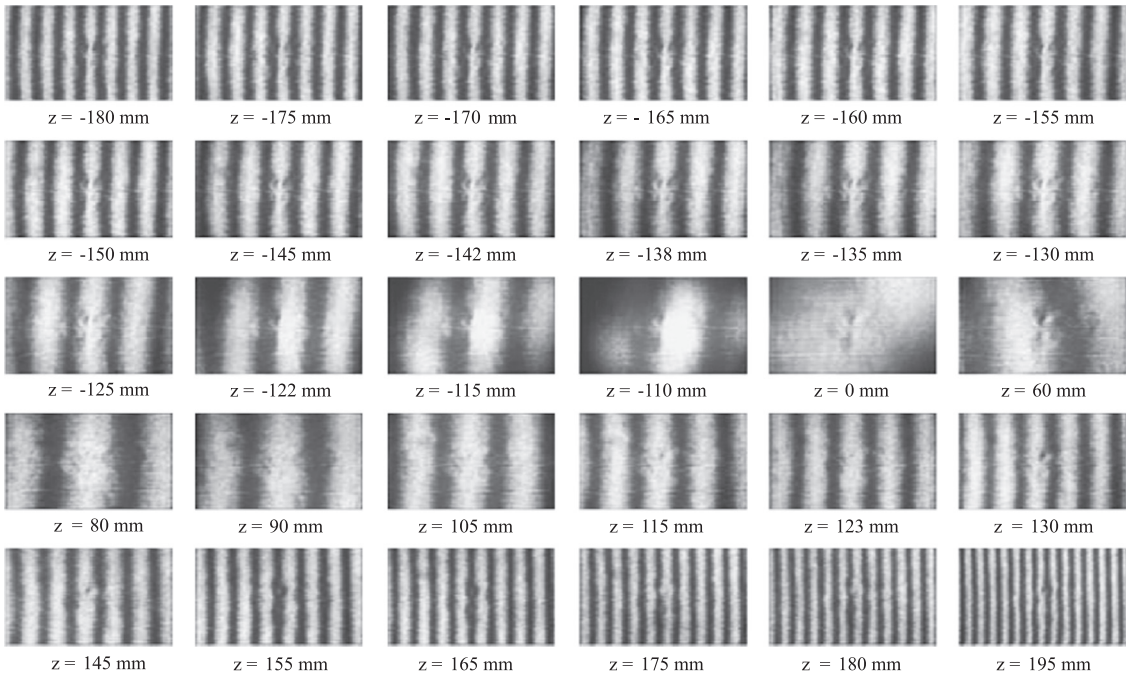

Fig. 2. Typical moiré patterns recorded at different distances of the sample from the focal plane of the first lens. The sample was a 40X objective with a commercial focal length of 4 mm.

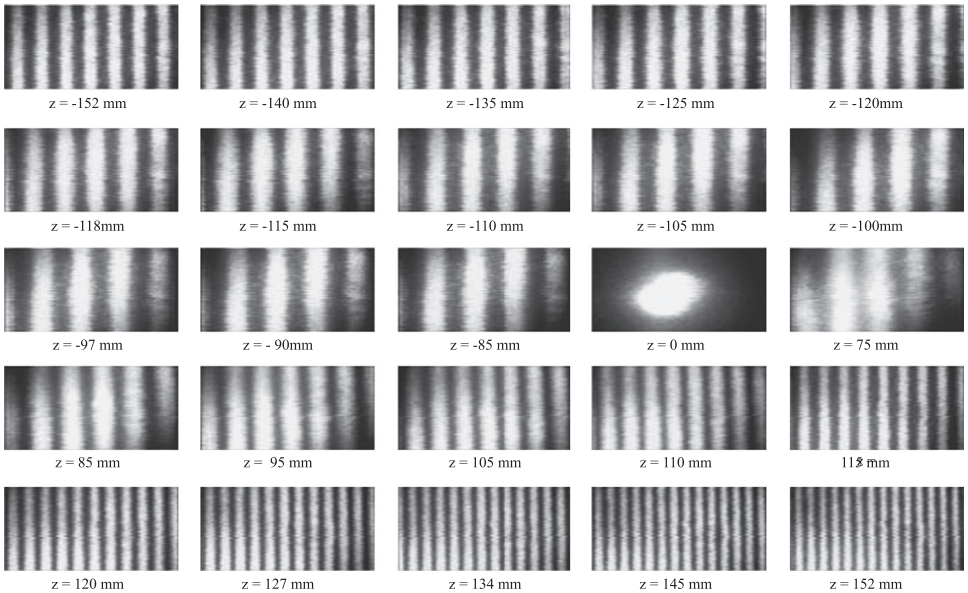

Fig. 3. Typical moiré patterns recorded at different distances of the sample from the focal plane of the first lens. The sample was a microlens with a commercial focal length of 16 mm.

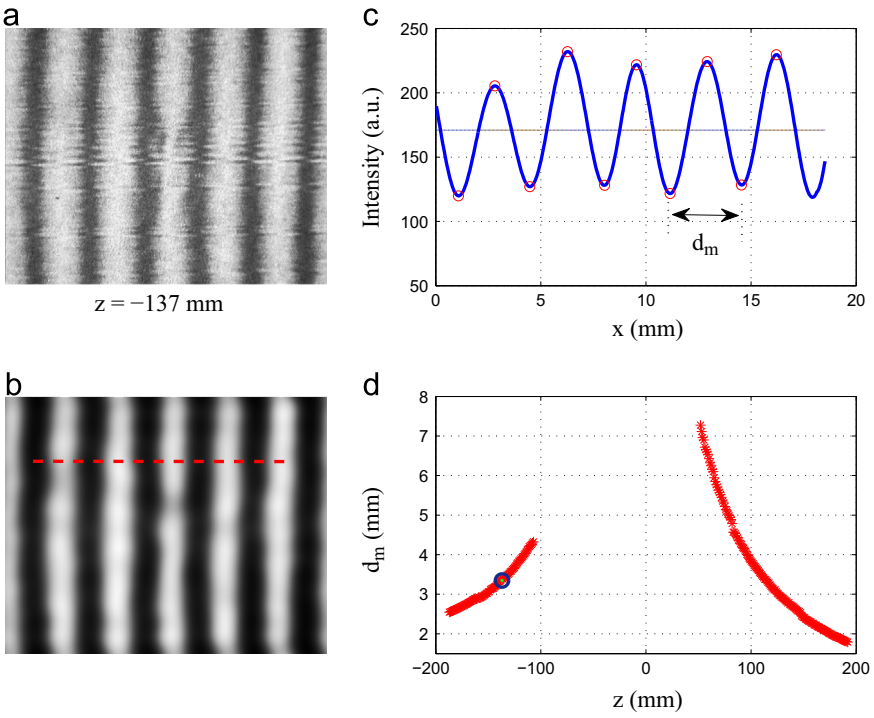

Fig. 4. (a) A typical moiré pattern at a given z, (b) corresponding to low-frequency illumination distribution, (c) intensity profile along the dashed red line illustrated in (b), and calculated moiré fringe period at the given z is shown by a blue circle in (d). Other data points in (d) correspond to other values of z. All the data are for a typical 40X objective with a commercial focal length of 4 mm. The corresponding video can be observed in the background (Media 1, MP4 Movie File, 3.01 MB). (For interpretation of the references to color in this figure caption, the reader is referred to the web version of this article.)

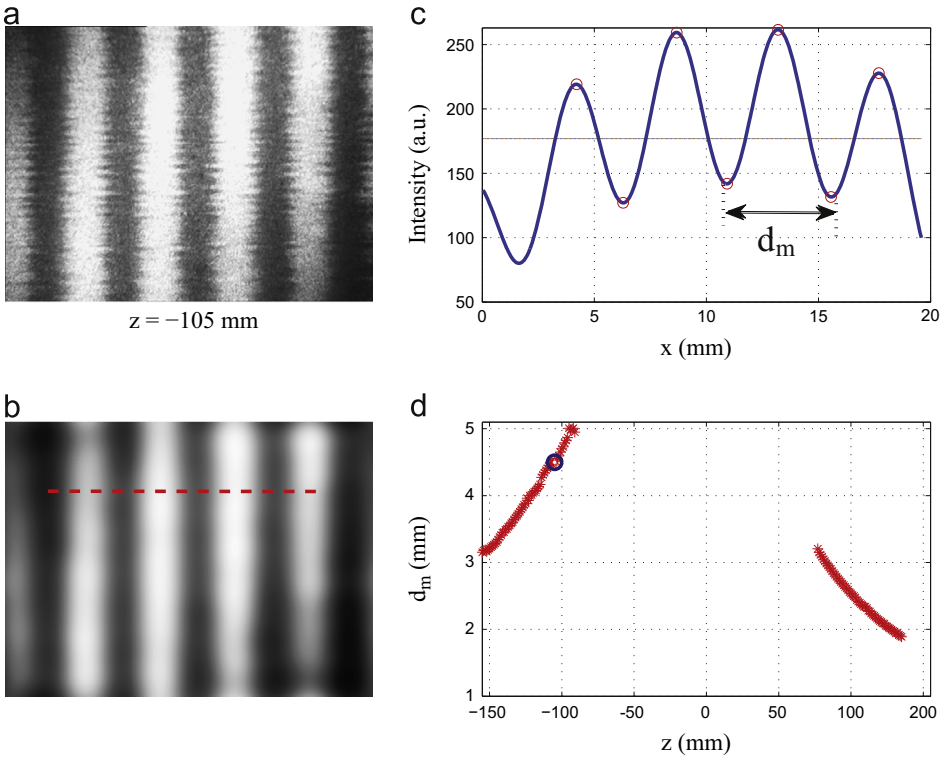

Fig. 5. (a) A typical moiré pattern at a given z, (b) corresponding to low-frequency illumination distribution, (c) intensity profile along the dashed red line illustrated in (b), and calculated moiré fringe period at the given z is shown by a blue circle in (d). Other data points in (d) correspond to other values of z. All the data are for a microlens with a commercial focal length of 16 mm. The corresponding video can be observed in the background (Media 2, MP4 Movie File, 1.85 MB). (For interpretation of the references to color in this figure caption, the reader is referred to the web version of this article.)

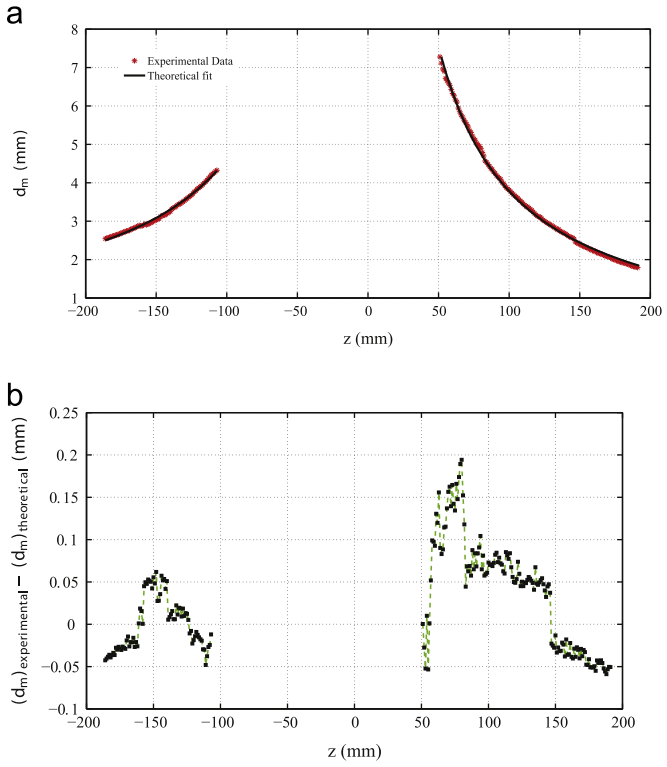

Fig. 6. (a) Behavior of moiré fringes period at various z, and theoretical fit on the experimental data for a 40X objective with a commercial focal length of 4 mm. The differences between theoretical model and experimental data are shown in (b).

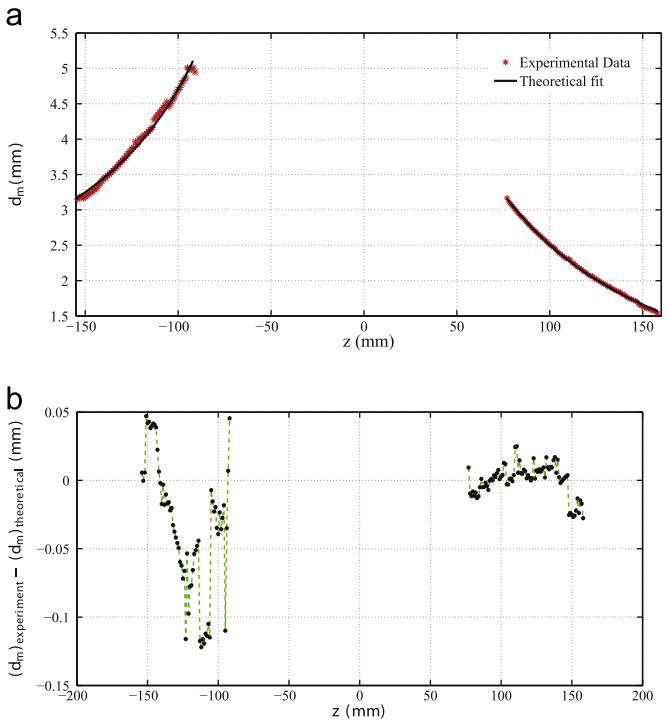

Fig. 7. (a) Behavior of moiré fringes period at various z, and theoretical fit on the experimental data for a microlens with a commercial focal length of 16 mm. The differences between theoretical model and experimental data are shown in (b).

of f_{ob}=4.06 mm and f_{ml}=16.02 mm are obtained for the 40X objective and microlens by the method, respectively.

It should be noted that in Figs. 4 and 7 which show the moiré period as a function of z there are gaps because the maximum measurable moiré period is limited by the size of the second grating.

We have applied the method to different microlenses and objective lenses to determine their focal lengths. For the mentioned experimental values of f_2, f_1, Z_k, L, and d, the obtained value of focal lengths are given in Table 1.

It is worth mentioning that the presented method is applicable to ordinary lenses with focal lengths of the order of about a meters with the given parameters of the setup, but for very long focal lengths, it seems that this method is not sensitive enough.

4. Error analysis

To obtain an estimation of the effective focal length measurement error, let us rewrite Eq. (7) in the following form:

$$f_{ml} = \frac{z^2}{f_2}\left(\frac{L}{f_2}-1\right) + \frac{z d f_2^2 \mp z^2 Z_k d_m}{d f_2^2}. \tag{8}$$

The uncertainty or error in the effective focal length measurement can be found by using the rules of propagation of uncertainties. If the original uncertainties are independent and random, the uncertainties are added in quadrature [24].

The uncertainty in the measurement of f_{ml} is originated from the uncertainties in the measurement of δz, δZ_k, δf_2, δL, δd, and δd_m which we denote by $(\delta f_{ml})_z$, $(\delta f_{ml})_{Z_k}$, $(\delta f_{ml})_{f_2}$, $(\delta f_{ml})_L$, $(\delta f_{ml})_d$, and $(\delta f_{ml})_{d_m}$, respectively. The uncertainty in f_{ml} due to δz alone, which we denote by $(\delta f_{ml})_z$ is

$$(\delta f_{ml})_z = (\text{error in } f_{ml} \text{ due to } \delta z \text{ alone}),$$

$$(\delta f_{ml})_z = \left|\frac{\partial f_{ml}}{\partial z}\right|\delta z,$$

$$(\delta f_{ml})_z = \left(\left|\frac{2zL}{f_2^2}\right| + \left|\frac{2z}{f_2}\right| + \left|\frac{2zZ_k d_m}{d f_2^2}\right| + 1\right)\delta z. \tag{9}$$

Similarly, the uncertainties in f_{ml} due to δf_2, δL, δd, δd_m, and δZ_k are

$$(\delta f_{ml})_{f_2} = \left(\frac{2z^2 L}{f_2^3} + \frac{z^2}{f_2^2} + \frac{2z^2 Z_k d_m}{d f_2^3}\right)\delta f_2,$$

$$(\delta f_{ml})_L = \left(\frac{z^2}{f_2^2}\right)\delta L,$$

$$(\delta f_{ml})_d = \left(\frac{z^2 Z_k d_m}{d^2 f_2^2}\right)\delta d,$$

$$(\delta f_{ml})_{d_m} = \left(\frac{z^2 Z_k}{d f_2^2}\right)\delta d_m,$$

$$(\delta f_{ml})_{Z_k} = \left(\frac{z^2 d_m}{d f_2^2}\right)\delta Z_k, \tag{10}$$

where δ shows the measuring error of the corresponding parameter, for example, δZ_k and δd_m are the reading error of the Talbot

Table 1
Measured values of the focal length of different microlenses and objectives and corresponding calculated errors by using the rules of propagation of uncertainties.

Number	Name of microlens or objective	Reported f (mm)	Measured f (mm)	Error (%)
1	100X objective	1.6	1.66 ±0.08	5.1
2	40X objective	4	4.06 ±0.05	1.1
3	20X objective	9	8.99 ±0.37	4.1
4	10X objective	20	20.07 ±0.76	3.8
5	4X objective	40	40.09 ±0.64	1.6
6	3.2X objective	50	49.90 ±1.6	3.2
8	Microlens 4	4	4.08 ±0.17	4.3
9	Microlens 8	8	8.03 ±0.33	4.1
10	Microlens 16	16	16.02 ±0.45	2.8

distance and the moiré fringe period, respectively. Finally, the total uncertainty in f_{ml} is a quadratic sum of these six partial uncertainties:

$$\delta f_{ml} = \sqrt{(\delta f_{ml})_z^2 + (\delta f_{ml})_{f_2}^2 + (\delta f_{ml})_L^2 + (\delta f_{ml})_d^2 + (\delta f_{ml})_{d_m}^2 + (\delta f_{ml})_{Z_k}^2}. \quad (11)$$

In order to achieve high precision, all of the quantities and their errors should be measured with possible high resolution. We need to know the uncertainties in each of the factors in the expression of Eq. (8) used to calculate f_{ml}. For the mentioned typical measurement for a 40X objective lens, according to Fig. 6, at points of $z=192$ mm and $z=52$ mm, we have minimum and maximum values of the period of moiré fringes, respectively. Therefore, the relative error, $\delta f_{ml}/f_{ml}$, for the measurement at point $z=192$ mm, for the experimental values $d_m=1.84$ mm, $\delta L=1$ mm, $\delta z=0.005$ mm, $\delta Z_k=1$ mm, $\delta d=$ negligible *is* 1.3% and for value of $z=52$ mm we have $d_m=7.27$ mm and the relative error is again 1.3%. It should be mentioned that in the experiment, z is scanned by the step motor with a step size of 1/200 mm and δd_m is equal to the length covered by a pixel on the moiré pattern that is equal 0.04 mm. Also, in this work we have determined moiré fringes period with one pixel accuracy, but it is possible to enhance this accuracy by using a sub-pixel algorithm [25]. For all of the experimental data, a mean value of the relative error of 1.1% is obtained.

For all of the reported measurements in Table 1, error analysis were carried out and corresponding relative error of the experiments are reported in the table. The maximum value of the relative error is 5.1% for a 100X objective lens of focal length 1.6 mm.

5. Conclusions

In this paper we demonstrated a new, simple, and fully automated method for measuring the effective focal length of microlenses. We employed parallel moiré deflectometry to measure the radius of curvature of the laser beam induced by the microlens under test. The microlens is moved along the optical axis of the setup and a graph of moiré period as a function of its position is obtained in a sensitive way. The focal length of the microlens is obtained from the moiré fringe period graph. Measurement error was determined in a range from 1.1% to 5.1% for a set of microlenses and objectives with different focal lengths from 1.6 mm to 50 mm. The implementation of the method is straightforward. In this method, knowing the position of the principal planes of the microlens is not needed. It can be employed to determine the small focal length of a small microlens without any limitation on its size. Also, it is applicable to an array of microlenses using a suitable lateral array displacer on the optical axis.

Acknowledgments

The authors would like to thank M.H. Hasanloo for some useful help in measurement of the samples. Also, the authors thank B. Farnudi for the linguistic editing of the paper and the anonymous referees for their constructive comments.

Appendix A. Supplementary material

Supplementary data associated with this article can be found in the online version of http://dx.doi.org/10.1016/j.optlaseng.2013.05.012.

References

[1] Popovic CD, Sprague RA, Connell GAN. Techniques for monolithic fabrication of microlens arrays. Appl Opt 1988;27:1281–4.
[2] Karp JH, Tremblay EJ, Ford JE. Planar micro-optic solar concentrator. Opt Express 2010;18:1122–33.
[3] Charriere F, Kühn J, Colomb T, Montfort F, Cuche E, Emery Y, et al. Characterization of microlenses by digital holographic microscopy. Appl Opt 2006;45:829–35.
[4] Miyashita T, Kato M, Ohta J. Wavefront aberration measurement technology for microlenses using a Mach–Zehnder interferometer with effective apertures. Opt Eng 2009;48:073609.
[5] Reichelt S, Zappe H. Combined Twyman–Green and Mach–Zehnder interferometer for microlens testing. Appl Opt 2005;44:5786–92.
[6] Kim M, Scharf T, Herzig HP. Small-size microlens characterization by multi-wavelength high-resolution interference microscopy. Opt Express 2010;18:14319–29.
[7] Alma A, Camacho P, Solano C, Cywiak M, Martnez-Ponce G, Baltazar R. Method for the determination of the focal length of a microlens. Opt Eng 2000;39:2149–52.
[8] Cywiak M, Servn M, Mendoza Santoyo F. Vibrating knife-edge technique for measuring the focal length of a microlens. Appl Opt 2001;4:4947–52.
[9] Buttner A, Zeitner UD. Calculation of the average lenslet shape and aberrations of microlens arrays from their far-field intensity distribution. Appl Opt 2002;41:6841–8.
[10] Sheik-bahae M, Said AA, Van Stryland EW. High-sensitivity, single-beam n_2 measurements. Opt Lett 1989;14:955–7.
[11] Abdelaziez Y, Banerjee P. A simple focal-length measurement technique for adaptive microlenses using Z-scan. Proc SPIE 2004;5523:256–63.
[12] de Angelis M, De Nicola S, Ferraro P, Finizio A, Pierattini G, Hessler T. An interferometric method for measuring short focal length refractive lenses and diffractive lenses. Opt Commun 1999;160:5–9.
[13] Bernardo LM, Soares ODD. Evaluation of the focal distance of a lens by Talbot interferometry. Appl Opt 1988;27:296–301.
[14] Malacara-Doblado D, Salas-Peimbert DP, Trujillo-Schiaffino G. Measuring the effective focal length and the wavefront aberrations of a lens system. Opt Eng 2010;49(1–5):053601.
[15] Pomarico JA, Torroba RD. Focal lengths measurements using digital speckle interferometry. Opt Commun 1997;141:1–4.
[16] Konno H, Ohara H, Muratai K, Nakan Y. Measurement of focusing properties of axially asymmetric lenses using moiré technique. Opt Rev 1994;1:107–9.
[17] Prakash S, Singh S, Verma A. A low cost technique for automated measurement of focal length using Lau effect combined with moiré readout. J Mod Opt 2006;53:2033–42.
[18] Wu Jia-jie, Chen Jia-bi, Xu An-cheng, Gao Xiao-yan, Zhuang Songlin. Focal length measurement based on Hartmann–Shack principle. Optik 2012;123:485–8.
[19] Rasouli S, Tavassoly MT. Application of the moiré deflectometry on divergent laser beam to the measurement of the angle of arrival fluctuations and the refractive index structure constant in the turbulent atmosphere. Opt Lett 2008;33:980–2.
[20] Rasouli S, Dashti M, Ramaprakash AN. An adjustable, high sensitivity, wide dynamic range two channel wave-front sensor based on moiré deflectometry. Opt Express 2010;18:23906–15.
[21] Rasouli S, Ghasemi H, Tavassoly MT, Khalesifard HR. Application of the parallel moiré deflectometry and the single beam Z-scan technique in the measurement of the nonlinear refractive index. Appl Opt 2011;50:2356–60.
[22] Patorski K. Handbook of the moiré fringe technique. Elsevier; 1993.
[23] Pedrotti FL, Pedrotti LS. Introduction to optics. Prentice Hall; 1993.
[24] Taylor JR. An introduction to error analysis the study of uncertainties in physical measurements, ISBN 0-935702-42-3 (cloth).- ISBN 0-935702-75-X (pbk.). Sausalito, California: University Science Books; 1997.
[25] Dashti M, Rasouli S. Measurement and statistical analysis of the wavefront distortions induced by atmospheric turbulence using two-channel moiré deflectometry. J Opt 2012;14:095704.